Geomechanics and Engineering, *Vol. 34, No. 2 (2023) 187-195*
https://doi.org/10.12989/gae.2023.34.2.187

Static and quasi-static slope stability analyses using the limit equilibrium method for mountainous area

Hosung Shin*

Department of Civil and Environmental Engineering, University of Ulsan, Daehak-ro 93, Nam-Gu, Ulsan 44610, Republic of Kiorea

(*Received June 16, 2022, Revised March 31, 2023, Accepted June 12, 2023*)

Abstract. Intensive rainfall during the summer season in Korea has triggered numerous devastating landslides outside of downtown in mountainous areas. The 2D slope stability analysis that is generally used for cut slopes and embankments is inadequate to model slope failure in mountainous areas. This paper presents a new 3D slope stability formulation using the global sliding vector in the limit equilibrium method, and it uses an ellipsoidal slip surface for static and quasi-static analyses. The slip surface's flexibility of the ellipsoid shape gives a lower FS than the spherical failure shape in the Fellenius, Bishop, and Janbu's simplified methods. The increasing sub-columns of each column tend to increase the FS and converge to a steady value. The symmetrical geometric conditions of the convex turning corners do not indicate symmetrical failure of the surface in 3D analysis. Pseudo-static analysis shows that the horizontal seismic force decreases the FS and increases the mass volume at the critical failure state. The stability index takes the FS and corresponding sliding mass into consideration to assess the potential risk of slope failure in complex mountainous terrain. It is a valuable parameter for selecting a vulnerable area and evaluating the overall risk of slope failure.

Keywords: ellipsoidal slip surface; global sliding vector; limit equilibrium method; three-dimensional slope stability analysis

1. Introduction

The accurate assessment of slope stability has attracted significant attention due to its impact on loss of life and property damage. Limit analysis for the slope stability is a plastic bounding theorem used to reduce the difference between a lower bound solution from a statically admissible stress field and an upper bound solution from a kinematically admissible velocity field (Chen and Scawthorn 1968). It is valuable to set both bounds to an exact solution. However, its practical application is very limited to simple geometric configurations due to numerical difficulties, especially with the lower bound solution (Deusdado *et al*. 2016, Donald and Chen 1997, Li *et al.* 2009). Still, it has difficulties analyzing mountainous regions and building hazard maps for landslides, like the strength reduction method using Finite Element Analysis (Ji 2014, Naeij *et al.* 2021).

Alternatively, limit equilibrium analysis has been the most popular method used for slope stability analysis. Since normal and tangential stresses acting on the selected slip surface are indeterminate, appropriate assumptions for the inter-slice forces are crucial to the global Factor of Safety (FS) from force equilibrium equations. Despite this shortcoming, limit equilibrium analysis can be used to analyze complex soil profiles, various shear strength models, seepage, the failure surface, and structural reinforcement (Ahmed et al. 2012; Dong-ping *et al.* 2017, Krahn 2003, Lim *et al.* 2016, Pantelidis *et al*. 2020, Yu *et al.* 1998). Slope stability analyses have primarily been performed for 2D (two-dimensional) cut slopes and embankments. FS from 2D analysis is a conservative estimation because the end edge of the failure surface in 3D analysis increases the shear resistance to reduce the FS. The recent difficulty in slope stability analysis of mountainous territory is based on the use of 1D slope analysis (infinite slope) for landslide susceptibility mapping rather than 3D analysis (Baum *et al.* 2008, Kim *et al*. 2014, Meisina and Scarabelli 2007, Michel *et al.* 2014).

The pseudo-static approach is the most common procedure employed for seismic slope stability evaluation in engineering practice, where an equivalent static force represents earthquake effects (Bray and Travasarou 2009, Lee *et al.* 2015). However, it has the disadvantage of simplifying a constant force in only one direction for the time-varying seismic load. Stability charts from limit analysis provide the preliminary assessment of slope safety (Baker *et al.* 2006, Gao *et al.* 2013, Michalowski and Martel 2011, Rao *et al*. 2021). Engineering practices call for the FS and yield acceleration to predict landslide probability (Jibson 2011, Kim and Sitar 2004).

This paper presents new succinct limit equilibrium formulations for the 3D slope stability. It also addresses pseudo-static stability analysis under horizontal seismic conditions. The developed method is applied to compare with published results, and this study deals with the field investigation of 3D slope stability of the mountainous area.

*Corresponding author, Professor
E-mail: shingeo@ulsan.ac.kr

ISSN: 2005-307X (Print), 2092-6219 (Online)

2. Formulation of the 3D limit equilibrium method

2.1 Ellipsoid failure surface

The 3D stability analysis determines the critical slip surface to obtain the minimum FS from a series of trial slip surfaces. This paper uses a general ellipsoidal geometry for the slip surface to provide flexibility to the failure shape (Fig. 1(a)).

$$f(\underline{p}) = \left[\underline{R} \bullet (\underline{p} - \underline{p}_c)\right]^T \bullet \underline{A} \bullet \left[\underline{R} \bullet (\underline{p} - \underline{p}_c)\right] - 1 = 0 \qquad (1)$$

where an operator • stands for matrix multiplication. The vector $\underline{p}(x, y, z)$ indicates a point on the ellipsoid and $\underline{p}_c(x_c, y_c, z_c)$ is the center point for an ellipsoid. a, b, and c are the ellipsoid radii to build the $\underline{A}$ matrix, and $\underline{n}^1(n_x^1, n_y^1, n_z^1)$, $\underline{n}^2$ and $\underline{n}^3$ (= $\underline{n}^1 \times \underline{n}^2$) are the rotated unit vectors of 3 axes of the ellipsoid in the x, y, and z global coordinates to build the $\underline{R}$ matrix as follows

$$\underline{A} = \begin{bmatrix} 1/a^2 & 0 & 0 \\ 0 & 1/b^2 & 0 \\ 0 & 0 & 1/c^2 \end{bmatrix}, \quad \underline{R} = [\underline{n}^1\ \underline{n}^2\ \underline{n}^3] = \begin{bmatrix} n_x^1 & n_x^2 & n_x^3 \\ n_y^1 & n_y^2 & n_y^3 \\ n_z^1 & n_z^2 & n_z^3 \end{bmatrix} \qquad (2)$$

The failure mass of the 3D slope is divided into a number of columns. Fig. 1(b) shows the outward normal vector of the bottom plane $\underline{n}^p$ of each column. The following equation gives the $\underline{n}^p$ vector for the ellipsoid shape

$$\begin{aligned} \underline{n}^p &= \hat{u}\left(\partial f/\partial x, \partial f/\partial y, \partial f/\partial z\right)^T \\ \partial f/\partial x &= 2\underline{n}^{1T} \bullet \underline{A} \bullet \left[\underline{R} \cdot (\underline{p} - \underline{p}_c)\right] \\ \partial f/\partial y &= 2\underline{n}^{2T} \bullet \underline{A} \bullet \left[\underline{R} \cdot (\underline{p} - \underline{p}_c)\right] \\ \partial f/\partial z &= 2\underline{n}^{3T} \bullet \underline{A} \bullet \left[\underline{R} \cdot (\underline{p} - \underline{p}_c)\right] \end{aligned} \qquad (3)$$

where $\hat{u}(v)$ denotes the unit vector in direction v.

Fig. 1(b) shows two vector components on the bottom of each column. $\underline{n}^d$ is the deepest direction of the bottom plane from $\underline{n}^p$, which is the same as the dip direction of the fracture plane in rock mechanics. $\underline{n}^s$ is the normal vector to the local sliding plane from a vector cross product of $\underline{n}^d$ and $\underline{n}^p$.

$$\begin{aligned} \underline{n}^d &= \hat{u}\left(n_x^p \cdot n_z^p, n_y^p \cdot n_z^p, -(n_x^{p2} + n_y^{p2})\right)^T \\ \underline{n}^s &= \hat{u}\left(\underline{n}^d \times \underline{n}^p\right) \end{aligned} \qquad (4)$$

The global sliding vector $\bar{\underline{n}}^s$ is the overall averaged vector for the products of the bottom area (A_s) and sliding vector $\underline{n}^s$ of each column, and it is normal to the global sliding plane.

$$\bar{\underline{n}}^s = \frac{\sum_{(i,j)} \underline{n}^s A_s}{\sum_{(i,j)} A_s} \qquad (5)$$

The global sliding vector $\bar{\underline{n}}^s$ indicates the central axis of the sliding slip surface. In the 2D slope stability, global and local sliding vectors are in the same direction perpendicular to the 2D plane.

Limit equilibrium analyses use the force equilibrium or moment equilibrium of 3D columns. This statically indeterminate problem requires additional assumptions on the interfacial forces between columns.

2.2 Moment equilibrium method

The moment equilibrium equation for the assemblage of all of the columns gives the ratio of resistance force to driving force for the failure surface to compute FS as follows

$$FS = \frac{\sum r \cdot [c \cdot A_l + (N - u \cdot A_l) \cdot \tan(\phi)]}{\sum r \cdot [\underline{W}^{gT} \bullet \underline{n}^d \cdot < \underline{n}^s \bullet \bar{\underline{n}}^s >]} \qquad (6)$$

where r is the distance between the center of the column bottom and the centroid of the ellipsoid, and N and u are the normal force and the average pore water pressure acting on the bottom of the column, respectively. The resultant shear force acting on the bottom face is assumed to be parallel with the dip direction of the column. In that case, the driving force is evaluated from the self-weight of the column $\underline{W}^g = W \cdot (0,0,-1)^T$ and its adjustment by $\underline{n}^d$ in the denominator of Eq. (6). The mismatch between the local and global sliding directions adjusts the driving shear force as follows: ($\underline{W}^{gT} \bullet \underline{n}^d = -W \cdot n_z^d$) by $< \underline{n}^s \bullet \bar{\underline{n}}^s > = sign(\underline{n}^{sT} \bullet \bar{\underline{n}}^s) \cdot \sqrt{\left| \underline{n}^{sT} \bullet \bar{\underline{n}}^s \right|}$. Therefore, the only unknown in Eq. (6) is the normal force N acting on the bottom of each column.

Fig. 1(c) presents interfacial forces acting on the vertical planes of the single column. E_x^1 and E_x^2 are the normal forces acting on both vertical interfaces between columns in the x-direction; and E_y^1 and E_y^2 are the normal forces in the y-direction. P_x is the shear force acting on both vertical interfaces between columns in the y-direction. V is the shear force acting on column faces in the z-direction.

The Fellenius method neglects the shear and normal forces acting on all of the vertical interfaces between columns ($\sum E = \sum P = \sum V = 0$ in Fig. 1(c)). So, the normal force acting is $N = \underline{W}^g \bullet \underline{n}^p = -W \cdot n_z^p$, and FS_F can be calculated from Eq. (6).

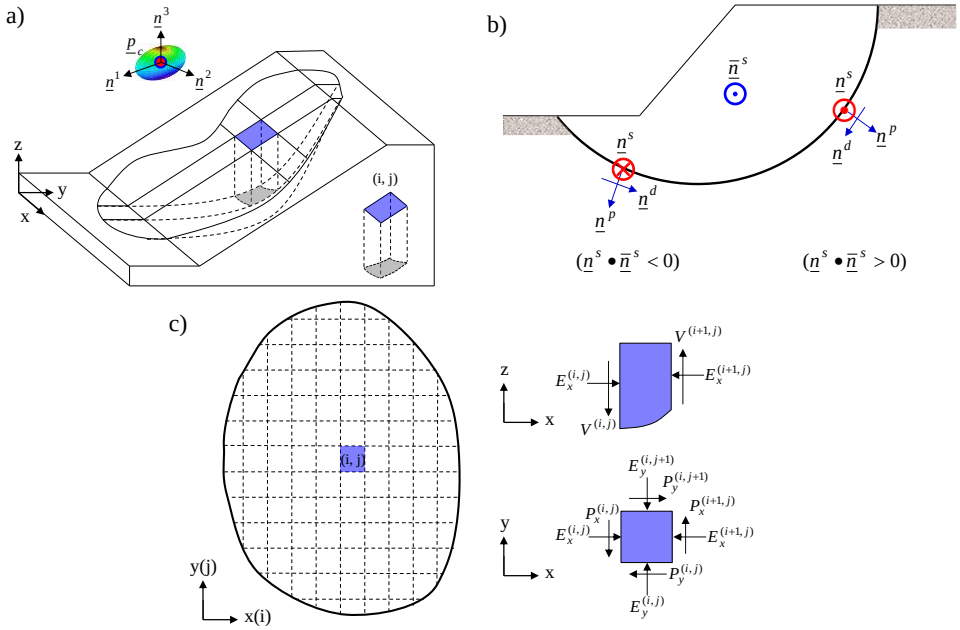

Fig. 1 Column-based slope model with ellipsoidal slip surface. (a) Ellipsoid for slip surface, (b) Sign convention for the local and global sliding vector, and (c) Planar view of divided columns and acting forces on the single column

$$FS_F = \frac{\sum r \cdot [c \cdot A_l - (W \cdot n_z^p + u \cdot A_l) \cdot \tan(\phi)]}{\sum r \cdot [-W \cdot n_z^d \cdot < \underline{n}^s \bullet \underline{\bar{n}}^s >]} \tag{7}$$

The Bishop method assumes that the vertical shear forces on the columns interfaces are in equilibrium ($\sum V = 0$), so the vertical force equilibrium of each column is given by the following equation

$$\begin{aligned} W &= -n_z^d \cdot T - n_z^p \cdot N \\ &= -n_z^d \cdot \frac{[c \cdot A_l - (W \cdot n_z^p - u \cdot A_l) \cdot \tan(\phi)]}{FS_B} - n_z^p \cdot N \end{aligned} \tag{8}$$

Rearrangement of the equation noted above gives the normal force N acting on the bottom of the column.

$$N = \frac{1}{\alpha}[W + \frac{n_3^d}{FS_B}\{c \cdot A_l - (u \cdot A_l \cdot \tan(\phi)\}] \tag{9}$$

where $\alpha = -n_z^p - n_z^d \cdot \tan(\phi) / FS_B$.

Since $c \cdot A_l + (N - u \cdot A_l) \cdot \tan(\phi)$ is $\frac{1}{\alpha}[c \cdot A - u \cdot A \cdot \tan(\phi) + W \cdot \tan(\phi)]$, the FS_B for the Bishop method is simplified as the following formula

$$FS_B = \frac{\sum r \cdot [c \cdot A + (W - u \cdot A) \cdot \tan(\phi)] / \alpha}{\sum r \cdot [-W \cdot n_z^d \cdot < \underline{n}^s \bullet \underline{\bar{n}}^s >]} \tag{10}$$

An iteration procedure is required to find FS_B in the equation noted above, and Newton's iterative method shows very fast convergence. The slope of pure cohesive soils needs no iteration due to constant α.

2.3 Force equilibrium method

Janbu's simplified method neglects the shear forces acting on the vertical interface between columns similar to Bishop method. The following equation is the force equilibrium of the column in the deepest sliding direction (Fig. 1(c))

$$\begin{aligned} &\underline{W}^{gT} \bullet \underline{n}^d \cdot < \underline{n}^s \bullet \underline{\bar{n}}^s > \\ &= T - (E_x^{(i,j)} - E_x^{(i+1,j)}) n_x^d - (E_y^{(i,j)} - E_y^{(i,j+1)}) n_y^d \\ &\quad + (P_x^{(i,j)} - P_x^{(i+1,j)}) n_y^d + (P_y^{(i,j)} - P_y^{(i,j+1)}) n_x^d \end{aligned} \tag{11}$$

where T is the shear force in the deepest sliding direction ($\underline{n}^d$) on the bottom of each column.

Modification of the equation noted above gives a recursive formula

$$\begin{aligned} &\frac{(E_x^{(i,j)} - E_x^{(i+1,j)}) n_x^d + (E_y^{(i,j)} - E_y^{(i,j+1)}) n_y^d - (P_x^{(i,j)} - P_x^{(i+1,j)}) n_y^d - (P_y^{(i,j)} - P_y^{(i,j+1)}) n_x^d}{\sqrt{n_x^{d\,2} + n_y^{d\,2}}} \\ &= \frac{T}{\sqrt{n_x^{d\,2} + n_y^{d\,2}}} + \frac{W \cdot n_z^d \cdot < \underline{n}^s \bullet \underline{\bar{n}}^s >}{\sqrt{n_x^{d\,2} + n_y^{d\,2}}} \end{aligned} \tag{12}$$

In the left term of the Eq. 12, the summation of the normal and shear forces for all of the sliding columns converges to zero according to the following equation:

$$\sum T / \beta = \sum [-W \cdot n_z^d \cdot < \underline{n}^s \bullet \underline{\bar{n}}^s >] / \beta \tag{13}$$

where $\beta = \sqrt{n_x^{d\,2} + n_y^{d\,2}}$.

FS_J is the ratio of the shear strength $c \cdot A_l + (N - u \cdot A_l) \cdot \tan(\phi)$ to the acting shear stress on the column bottom

$$FS_J = \frac{\sum [c \cdot A_l + (N - u \cdot A_l) \cdot \tan(\phi)] / \beta}{\sum [-W \cdot n_z^d \cdot < \underline{n}^s \bullet \underline{\bar{n}}^s >] / \beta} \quad (14)$$

The vertical equilibrium of each column gives the normal force N acting on the column bottom as calculated in Eq. (9).

$$FS_J = \frac{\sum [c \cdot A + (W - u \cdot A) \cdot \tan(\phi)] / (\alpha \cdot \beta)}{\sum [-W \cdot n_z^d \cdot < \underline{n}^s \bullet \underline{\bar{n}}^s >] / \beta} \quad (15)$$

where $\alpha = -n_z^p - n_z^d \cdot \tan(\phi) / FS_J$.

2.4 Pseudo-static analysis

The pseudo-static approach is still the most common procedure for seismic slope stability analysis. It is an extension of limiting equilibrium analysis considering the earthquake load. An equivalent seismic force due to an earthquake is given as the product of a seismic coefficient k_h and the weight of the sliding mass. Newmark (1965) introduced the concept of yield acceleration k_y to make FS=1.0, and the permanent displacement by an earthquake is obtained by integrating the relative acceleration time history exceeding the yield acceleration.

The seismic force is parallel to the x and y components of the global sliding vector ($\underline{\bar{n}}^s$)

$$\underline{W}^E = k_h \cdot W \cdot \frac{(\bar{n}_x^s, \bar{n}_y^s, 0)^T}{\sqrt{\bar{n}_x^{s\,2} + \bar{n}_y^{s\,2}}} = k_h \cdot W \cdot \underline{n}^E \quad (16)$$

where k_h is the horizontal seismic acceleration coefficient.

The moment equilibrium equation for all of the assemblage of the columns is modified to include the equivalent seismic force as follows

$$FS = \frac{\sum r \cdot [c \cdot A_l + (N - u \cdot A_l) \cdot \tan(\phi)]}{\sum r \cdot [\underline{W}^g \bullet \underline{n}^d \cdot < \underline{n}^s \bullet \underline{\bar{n}}^s >] + a \cdot k_h \cdot W} \quad (17)$$

where a is the vertical distance between the centroid of the ellipsoid and the mass center of the column.

In the Fellenius method, the normal force N acting on the bottom plane of the column is modified to include horizontal seismic forces as follows:

$$N = (\underline{W}^g + \underline{W}^E) \bullet \underline{n}^p \quad (18)$$

The original formulation (Eq. (7)) is rewritten to include horizontal earthquake-induced acceleration coefficient k_h as follows:

$$FS_{FE} = \frac{\sum r \cdot [c \cdot A_l - (W \cdot n_z^p + u \cdot A_l - k_h \cdot W \cdot \underline{n}^E \bullet \underline{n}^p) \cdot \tan(\phi)]}{\sum r \cdot [-W \cdot n_z^d \cdot < \underline{n}^s \bullet \underline{\bar{n}}^s >] + a \cdot k_h \cdot W} \quad (19)$$

The yield acceleration k_{Fy} is the minimum acceleration needed to reduce the factor of safety to unity. By assigning unity to FS_{FE}, the equation can be rearranged in terms of the yield acceleration as follows:

$$k_{Fy} = \frac{\sum r \cdot [c \cdot A_l - (W \cdot n_z^p + u \cdot A_l) \cdot \tan(\phi) + W \cdot n_z^d \cdot < \underline{n}^s \bullet \underline{\bar{n}}^s >]}{\sum a \cdot W - r \cdot W \cdot \tan(\phi) \cdot \underline{n}^E \bullet \underline{n}^p} \quad (20)$$

The Bishop method assumes that the shear forces acting on the vertical column faces are in equilibrium so that the horizontal seismic forces have no effect on the normal force N acting on the bottom plane of the column.

$$FS_{BE} = \frac{\sum r \cdot [c \cdot A + (W - u \cdot A) \cdot \tan(\phi)] / \alpha}{\sum r \cdot [-W \cdot n_z^d \cdot < \underline{n}^s \bullet \underline{\bar{n}}^s >] + a \cdot k_h \cdot W} \quad (21)$$

The yield acceleration k_{By} for the Bishop method is a closed-form solution and thus no longer requires an iterative scheme as is necessary for the static Bishop method.

$$k_{By} = \frac{\sum r \cdot [c \cdot A + (W - u \cdot A) \cdot \tan(\phi)] / \alpha_c + r \cdot W \cdot n_z^d \cdot < \underline{n}^s \bullet \underline{\bar{n}}^s >]}{\sum a \cdot W} \quad (22)$$

where $\alpha_c = -n_z^p - n_z^d \cdot \tan(\phi)$.

In the Janbu method, the normal force N is given by the force equilibriums parallel to the bottom plane and the vertical force equilibrium of the column.

$$FS_{JE} = \frac{\sum [c \cdot A + (W - u \cdot A) \cdot \tan(\phi)] / (\alpha \cdot \beta)}{\sum [-W \cdot n_z^d \cdot < \underline{n}^s \bullet \underline{\bar{n}}^s > + k_h \cdot W] / \beta} \quad (23)$$

The yield acceleration k_{Jy} for the Janbu method is a direct solution with no iteration to compute.

$$k_{Jy} = \frac{\sum [c \cdot A + (W - u \cdot A) \cdot \tan(\phi)] / (\alpha_c \cdot \beta) + [W \cdot n_z^d \cdot < \underline{n}^s \bullet \underline{\bar{n}}^s >] / \beta}{\sum W / \beta} \quad (24)$$

3. Applications for three-dimensional slopes

3.1 Slope stability for one-sided slope

3.1.1 Homogeneous slope of purely cohesive soil

Fig. 2 shows a fixed spherical slip surface intersecting with cohesive soil. The constant shear strength along the slip surface gives a closed-form solution, FS=1.402 (Baligh and Azzouz 1975, Gens et al. 1988; Silvestri 2006). It constitutes a popular benchmark to evaluate various formulations of 3D slope stability (Table 1). The Bishop method using a spherical failure surface makes FS=1.405 and the volume 0.65m^3 (Fig. 2(a)). Fig. 2(b) shows the effects of each column's sub-division on FS in different models. The increase in the sub-columns of each column tends to increase the FS and converge to a steady value (Huang *et al.* 2002, Xie *et al.* 2006, opposite trend in Lam and Fredlund 1993). The Fellenius and Bishop methods give the same results for only cohesive soils due to no effects from the normal force N on the shear strength (comparable to Xie *et al*. 2006). Their estimates approached the closed-form solution as more of the columns were subdivided. The FS from the Janbu method is more sensitive to the cell size than those from the other methods.

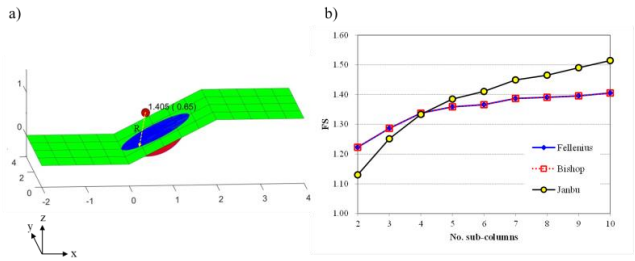

Fig. 2 A spherical failure surface in frictionless soil (R=1.0, 2:1 slope, γ=1.0, c=0.1, ϕ=0°). (a) Factor of safety and the volume in the Bishop model with 10 sub-divisions of each column, (b) Effects of the number of sub-divisions of each column on the FS in different models. Dimension of the rectangle on the slope=0.4 m(x)×1.0 m(y). The text in the figure represent FS (volume)

Table 1 Previous studies on homogeneous slopes of purely cohesive soil

Authors	Method	FS
Cheng and Yip (2007)	Limit equilibrium analysis	FS=1.39
Griffiths and Marquez (2007)	FE analyses	FS=1.39
Hungr *et al.* (1989)	Limit equilibrium analysis	FS=1.422
Lam and Fredlund (1993)	Limit equilibrium analysis	FS=1.386~1.472
Michalowski and Drescher (2009)	Limit analysis	FS= 1.402
Reid *et al.* (2015)	Limit equilibrium analysis	FS=1.40
Stianson *et al.* (2011)	Limit equilibrium analysis based on finite element method	FS=1.403
Xie *et al.* (2006)	Limit equilibrium analysis	FS=1.372~1.389

For only cohesive soils, no iteration is needed to compute FS in both the Bishop and Janbu methods.

3.1.2 Homogeneous slope of cohesive-frictional soil

Fig. 3 shows a comparative study of the 3D failure surface with a fixed centroid in a c-ϕ soils. Hungr *et al.* (1989) obtained an FS=1.23 for the critical ellipsoidal surface with an aspect ratio of R_2/R_1=0.66. For spherical failure surface, Xie *et al.* (2006) showed FS=1.180~1.222 from various methods and Pantelidis and Griffiths (2013) obtained FS=1.258. Numerical results using a spherical slip surface approach an asymptotic FS value with the column sub-divisions (Huang *et al.* 2002).

Fig. 3 shows the effects of a slip surface's flexibility on the FS; results using ellipsoid shapes give lower FS values than circular shapes in all of the methods. The Bishop method estimates higher FS values than the Fellenius method, and their difference converges to zero with an increasing number of sub-columns. However, the Janbu method predicts lower FS values than the Bishop method with a small number of sub-columns, but the result is reversed with a larger number of sub-columns. The Janbu

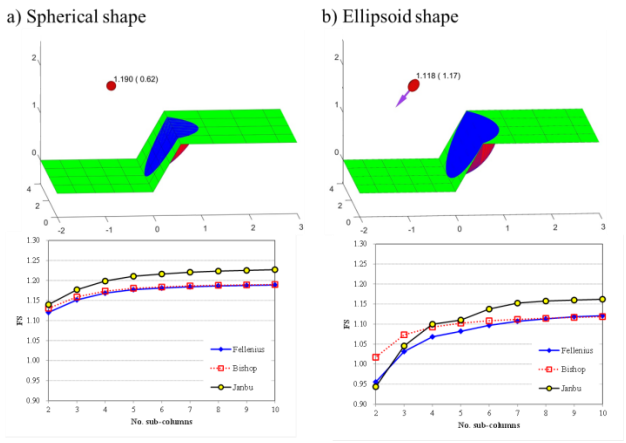

Fig. 3 The FS and effects of the number of sub-columns in each column on the failure surface with a fixed centroid (x_c=-0.7, z_c=1.9) (Hungr *et al.* 1989, x_c=-0.7, z_c=1.9) in cohesion-frictional soil (H=1.0, θ=60°, γ=1.0, c=0.116, ϕ=15°). (a) Spherical slip surface and (b) Ellipsoid slip surface

method is more sensitive to column discretization of the failure mass and shows slower convergence to a steady FS than the Bishop method.

3.2 Slope stability analysis of convex turning corners

Convex or concave corner slopes are common in embankments and cut slopes. Concave slopes provide more confinement from the two ends of the failure surface, while convex slopes have no confinement from the two ends (Camargo *et al.* 2016, Cheng *et al.* 2005). Therefore, convex slopes are more critical to slope failure than the concave slopes (Sun *et al.* 2017 using the strength-reduction method). The intersection of two straight slopes forms a convex turning corner, and the corner angle is equal to 90°.

In this study, the convex slope has a height of H=5 m, and the inclination angle to the horizontal is θ=45°. The soil properties are unit weight of γ=19.6 kN/m^3, cohesion of c=9.8 kPa, and friction angle of ϕ=30°. The ratio k_h of a_h/g is a dimensionless horizontal seismic acceleration coefficient, a_h/g, in the pseudo-static analysis. The 2D static stability analyses on the one-side slope (H=5 m, θ=45°) are the reference value for the 3D analysis. This study uses a trial procedure to find the critical slip surface, and the size and centroid location of slip surfaces are changed iteratively within a specific range (Xie *et al.* 2004).

In the static analysis, the 2D results (FS_{2D}) produces lower FS values than those for 3D convex corner slopes due to the end effects (Table 2). Fig. 4 shows the static analysis for the slope with convex turning. The symmetrical geometric conditions of convex turning corners do not locate the symmetrical slip surface associated with the minimum FS (Huang and Tsai 2000, Zhang *et al.* 2018).

The Bishop method yields higher FS values than the other two methods. The FS using the ellipsoid failure shape is lower than that using the spherical shape because of its geometric flexibility. Furthermore, 3D stability analyses produce the volume of the critical failure surface. In the

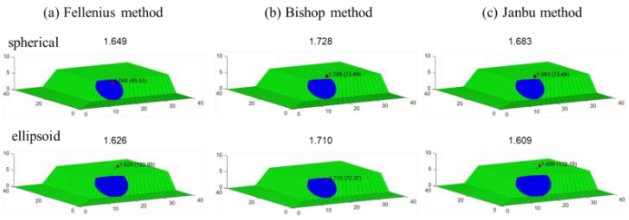

Fig. 4 Static stability results of a 3D slope with convex turning corners for critical spherical and ellipsoid shapes. Red arrows in the ellipsoid shape indicate the sliding direction

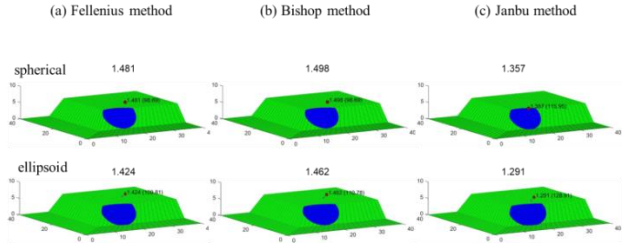

Fig. 5 Pseudo-static stability results of a 3D slope with convex turning corners for critical spherical and ellipsoid shapes (horizontal acceleration coefficient k_h=0.1)

Table 2 Static and pseudo-static analysis for 3D slopes with convex turning corners

Method		Fellenius		Bishop		Janbu	
		Spherical	Ellipsoid	Spherical	Ellipsoid	Spherical	Ellipsoid
Static	FS_{2D}	1.535	1.514	1.596	1.560	1.522	1.479
	FS_{3D}	1.649	1.626	1.728	1.710	1.683	1.609
	$V(m^3)$	89.83	103.95	73.49	72.38	73.49	122.15
Pseudo-static (k_h=0.1)	FS_{3D}	1.481	1.424	1.498	1.462	1.357	1.291
	$V(m^3)$	98.69	109.81	98.69	110.78	115.95	128.91
	k_y	0.546	0.439	0.418	0.361	0.247	0.227

Fellenius and Janbu methods, the ellipsoid shape estimates a larger volume than the spherical shape.

The critical failure shapes from the pseudo-static analysis are shown in Fig. 5 for different methods and slip surface shapes. The failure shapes at the critical FS are not symmetrical like those for the static analyses. The horizontal seismic force decrease the FS in the slope stability analysis, and the failure volume tends to increase in comparison to that in the static analysis (Table 2). In the pseudo-static analysis, the yield acceleration k_y to reach the failure state (FS=1) is directly related to FS, and the lower critical FS needs smaller yield acceleration. There is a large difference in the value of the yield acceleration depending on the analysis method.

3.3 Field application

The study area is located in a mountainous area of Ulsan Metropolitan City in South Korea. Ulju county designated it as a vulnerable area for landslides. It includes the Un-

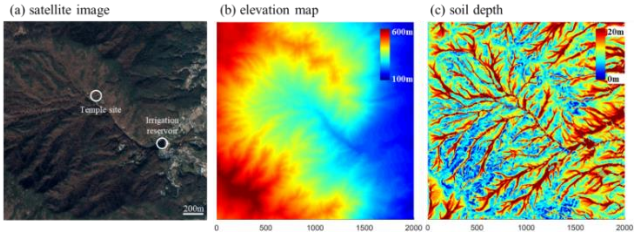

Fig. 6 Study area for the slope stability analysis. (a) Satellite image, (b) Elevation map and (c) Soil depth

Heung temple site (Ulsan Metropolitan City Monument No. 43, built in AD ~600) and several Buddhist sites in its lower sites. Two debris barriers near the temple site were installed due to sustained landslides in this area, and an irrigation reservoir is located downstream of the valley (Fig. 6(a)). Digital Elevation Model (DEM) from electric topographic maps is used to compute topographic indexes to characterize the land morphology.

The spatial distribution of soil depth arises from the complex interactions of topography, parent material, climate, and biological, chemical, and physical processes (Tesfa *et al.* 2009). Thus, soil depth can be expressed as a function of many different and interplaying factors, such as the underlying lithology, the slope gradient, the hillslope curvature, the upslope contributing area, and the vegetation cover. In this study, the S-model is modified to consider the specific catchment area (SCA) and slope angle (Saulnier *et al.* 1997) as follows

$$h = h_{\max} \cdot [1 - \beta_\theta \cdot (\tan(\theta) - \tan(\theta_{\min}))] \cdot [1 - \beta_{SCA} \cdot (\log(SCA_{\max}) - \log(SCA))] \quad (25)$$

where SCA is the total upslope catchment area draining across a unit length of contour (Moore *et al.* 1991). The scale factors for the slope angle and SCA can be calculated as $\beta_\theta = \frac{1 - h_{\min}/h_{\max}}{\tan(\theta_{\max}) - \tan(\theta_{\min})}$ and $\beta_{SCA} = \frac{1 - h_{\min}/h_{\max}}{\log(SCA_{\max}) - \log(SCA_{\min})}$, respectively. The parameters in this study are h_{max}=20 m, h_{min}=0.5 m (measured borehole data), θ_{max}=50°, θ_{min}=10°, SCA_{max}=10^4 m^2/m, and SCA_{min}=1 m^2/m.

The Bishop method is used to search for the critical failure surface with a spherical shape for 3D slope stability analysis of this complex mountainous territory. This study does not consider pore water pressure change with depth due to rainfall infiltration (Qi *et al.* 2014, Shin and Kim 2017, Tran *et al.* 2019). When the slip surface is deeper than the soil depth, the slip surface consists of a slip surface within the soil layer and the enclosed interface between the soil and the bedrock below. Pixel spacing is 5 m×5 m equal spacing, and OpenMP parallel programming is used to process 370 kilo-pixels for the study area of 3.075 km×3.0 km (Fig. 6). The soil properties used are unit weight γ=19.6 kN/m^3, cohesion c=9.8 kPa, and the friction angle ϕ=30°.

To visualize 3D stability analysis, the FS at each pixel indicates the minimum value from all of the trial failure shapes, which the centroid coincides with the 2D coordinate of the pixel.

Fig. 7(a) shows the numerical results of both static and pseudo-static slope stability analysis. The southwest area of

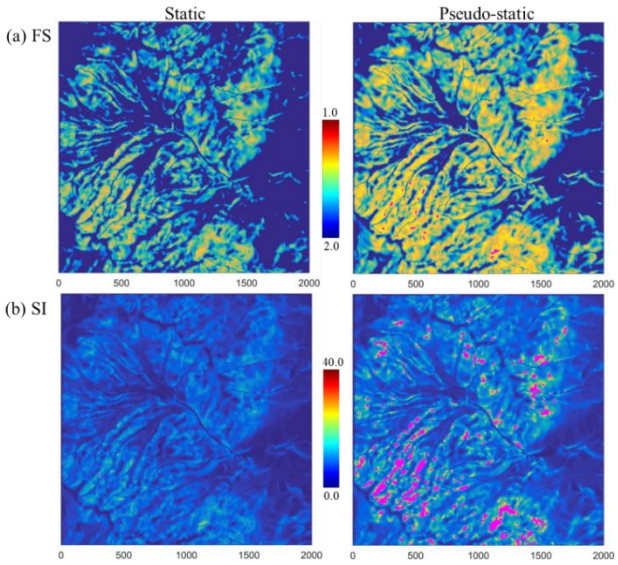

Fig. 7 3D slope stability results for the mountainous area of the Ulsan Metropolitan City in South Korea (Bishop method, k_h=0.1 for pseudo-static analysis)

the analysis domain has some pixels with low FS in the static analysis. Most slope failures in the southwest tend to geographically flow into the currently installed check dams in the central zone. However, landslides in the due south area could flow to the north-east and cause damage to the neighboring villages below the irrigation reservoir. Engineering measures are needed to mitigate the direct damage of landslides to the village. In the pseudo-static analysis, the seismic load increases the potential risk intensity of slope failure. The FS maps for both static and pseudo-static analysis provide a localized low FS region, but it is not apparent enough to designate the zone.

A stability index is proposed to consider FS and the corresponding failure volume, and it could be a quantitative scale of the slope failure. A high stability index indicates an increased risk due to slope failure as follows

$$S_I = \frac{1}{FS - FS_{ref}} \times \log\left(\frac{V}{V_{ref}}\right) \tag{26}$$

where the parameters used are FS_{ref}=1.0 and V_{ref}=1.0, and users can adjust these parameters to clarify the high-risk zone in the analysis domain. In Fig. 7(b), the stability index map based on the FS and the resulting failure volume is more appropriate for defining the hazardous area and evaluating the risk of landslides. These maps and values can help geotechnical engineers to delineate the border of a risk area for landslides.

Fig. 8(a) shows the FS histogram for all of the pixels in the study area. Results from the static analysis have a log-normal distribution (median=1.86, μ=0.05). The FS distribution from the pseudo-static analysis is shifted to the left in the log-normal curve (median=1.58, σ=0.05), and it produces a higher median than the static analysis. In the histogram of the stability index (Fig. 8(b)), the additional seismic force increases the stability index of the pixels (median=6.97, σ=0.48) compared to that of the static

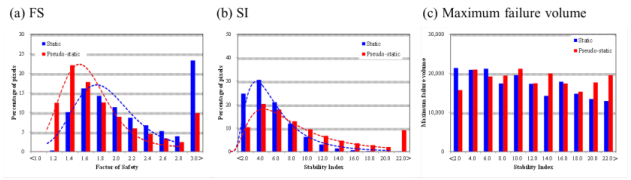

Fig. 8 Histogram of the entire pixels in the study area. (a) Histogram of FS, (b) Histogram of SI, and (c) Maximum failure volume at each SI interval

analysis (median=4.77, σ=0.39). The percentage of the pixels with a higher stability index than 20 is 0.147% in the static analysis and 9.13% in the seismic analysis. Fig. 8(c) shows the maximum failure volume for the pixels within the stability index intervals. The average failure volume for this study area is approximately 15,000~20,000 m^3. The pseudo-static analysis predicts more failure volume in the high-risk area (stability index > 20) than the static analysis.

4. Conclusions

This paper presents a new 3D slope stability formulation using the global sliding vector for a general ellipsoid failure surface. Based on the limit equilibrium method, moment equilibrium equations (Fellenius and Bishop methods) and force equilibrium equations (Janbu method) produces the FS of all of the assemblage of the columns. Newton's iteration procedure is required to determine the FS in the Bishop and Janbu methods. For pseudo-static analysis, additional seismic force is applied to the horizontal direction of the global slope sliding to obtain the FS for the critical failure surface. Computation of the yield acceleration k_c does not require iteration in all of the methods.

The following conclusions are drawn from the numerical study of 3D slopes:

- Homogeneous slope of purely cohesive soil: an increase in sub-columns tends to increase the FS and converge to a steady value;
- Homogeneous slopes of cohesive-frictional soil: Flexibility of the ellipsoidal slip surface produces lower FS than the spherical shape for all of the methods. The Bishop method always produced higher FS than the Fellenius method;
- Stability analysis of convex turning corners: the symmetrical convex corners of the slope cause a non-symmetrical failure surface. Pseudo-static analysis increases the failure volume at critical FS values compared to that in static analysis;
- Field application to a mountainous area: the stability index is proposed to take the FS and the corresponding failure volume into consideration to assess a quantitative scale of the slope failure. A stability index map helps to delineate the border of the hazardous areas for landslides;

In the complex mountainous terrain, 3D slope stability analysis is essential for the accurate analysis and subsequential debris flow analysis, which requires the triggering amount of the initial landslide. Comprehensive judgment of the FS and stability index is appropriate for selecting the vulnerable area and evaluating the overall risk for slope failure.

Acknowledgments

This research was supported by Research Funds from the National Research Foundation of Korea (KNRF-2022R1A2C200823612) and Korea Institute of Marine Science & Technology Promotion (KIMST-20220364).

References

Ahmed, A., Ugai, K. and Yang, Q. (2012), "Assessment of 3D slope stability analysis methods based on 3D simplified Janbu and Hovland methods", *Int. J. Geomech.*, **12**, 81-89. https://doi.org/10.1061/(ASCE)GM.1943-5622.0000117.

Baker, R., Shukha, R., Operstein, V. and Frydman, S. (2006), "Stability charts for pseudo-static slope stability analysis", *Soil Dyn. Earthq. Eng.*, **26**, 813-823. https://doi.org/10.1016/j.soildyn.2006.01.023.

Baligh, M.M. and Azzouz, A.S. (1975), "End effects on stability of cohesive slopes", *ASCE J. Geotech. Eng. Div.*, **101**(11), 1105-1117.

Baum, R.L., Savage, W.Z. and Godt, J.W. (2008), TRIGRS - A Fortran program for transient rainfall infiltration and grid-based regional slope-stability analysis, Version 2.0. U. S. Geological Survey.

Bray, J. and Travasarou, T. (2009), "Pseudostatic coefficient for use in simplified seismic slope stability evaluation", *J. Geotech. Geoenviron. Eng.*, **135**, 1336-1340. https://doi.org/10.1061/(ASCE)GT.1943-5606.0000012.

Camargo, J., Velloso, R. and Vargas, E. (2016), "Numerical limit analysis of three-dimensional slope stability problems in catchment areas", *Acta Geotechnica*, **11**(6), 1369-1383. https://doi.org/10.1007/s11440-016-0459-3.

Chen, W.F. and Scawthorn, C. (1968), Limit analysis and limit equilibrium solutions in soil mechanics. Fritz Laboratory Reports.

Cheng, Y.M., Liu, H., Wei, W. and Au, S. (2005), "Location of critical three-dimensional non-spherical failure surface by NURBS functions and ellipsoid with applications to highway slopes", *Comput. Geotech.*, **32**, 387-399. https://doi.org/10.1016/j.compgeo.2005.07.004.

Cheng, Y.M. and Yip, C. (2007), "Three-dimensional asymmetrical slope stability analysis extension of Bishop's, Janbu's, and Morgenstern-Price's Techniques", *J. Geotech. Geoenviron. Eng.*, **133**(12), 1544-1555. https://doi.org/10.1061/(ASCE)1090-0241(2007)133:12(1544).

Deusdado, N., Antão, A.N., Silva, M.V.D. and Guerra, N. (2016), "Application of the upper and lower-bound theorems to three-dimensional stability of slopes", *Procedia Eng.*, **143**, 674-681. https://doi.org/10.1016/j.proeng.2016.06.097.

Donald, I.B. and Chen, Z.Y. (1997), "Slope stability analysis by the upper bound approach: Fundamentals and methods", *Can. Geotech. J.*, **34**, 853-862. https://doi.org/10.1139/t97-061.

Dongping, D., Liang, L. and Zhao L. (2017), "LEM for stability analysis of 3D slopes with general-shaped slip surfaces", *Int. J. Geomech.*, **17**(10). https://doi.org/10.1061/(ASCE)GM.1943-5622.0000987.

Gao, Y., Zhang, F., Lei, G., Li, D., Wu, Y. and Zhang, N. (2013), "Stability charts for 3D failures of homogeneous slopes", *J. Geotech. Geoenviron. Eng.*, **139**, 1528-1538. https://doi.org/10.1061/(ASCE)GT.1943-5606.0000866.

Gens, A., Hutchison, J.N. and Cavounidis, S. (1988), "Three dimensional analysis of slopes in cohesive soils", *Géotechnique*, **38**(1), 1-23.

Griffiths, D.V. and Marquez, R.M. (2007), "Three-dimensional slope stability analysis by elasto-plastic finite elements", *Géotechnique*, **57**(6), 537-546. https://doi.org/10.1680/geot.2007.57.6.537.

Huang, C.C. and Tsai, C.C. (2000), "New method for 3D and asymmetrical slope stability analysis", *J. Geotech. Geoenviron. Eng.*, **126**, 917-927. https://doi.org/10.1139/cgj-2017-0317.

Huang, C.C., Tsai, C.C. and Chen, Y.H. (2002), "Generalized method for three dimensional slope stability analysis", *J. Geotech. Geoenviron. Eng.*, **128**(10), 836-848. https://doi.org/10.1061/(ASCE)1090-0241(2002)128:10(836).

Hungr, O., Salgado, F.M. and Byrne, P.M. (1989), "Evaluation of a three-dimensional method of slope stability analysis", *Can. Geotech. J.*, **26**(4), 679-686. https://doi.org/10.1139/t89-079.

Ji, J. (2014), "Sensitivity-based reliability analysis of earth slopes using finite element method", *Geomech. Eng.*, **6**(6), 545-560. https://doi.org/10.12989/gae.2014.6.6.545.

Jibson, R. (2011), "Methods for assessing the stability of slopes during earthquakes - A retrospective", *Eng. Geol.*, **122**, 43-50. https://doi.org/10.1016/j.enggeo.2010.09.017.

Kim, J., Jeong, S. and Bae, D. (2014), "GIS-based prediction method of landslide susceptibility using a rainfall infiltration-groundwater flow model", *Eng. Geol.*, **182**, 63-78. https://doi.org/10.1016/j.enggeo.2014.09.001.

Kim, J. and Sitar, N. (2004), "Direct estimation of yield acceleration in slope stability analyses", *J. Geotech. Geoenviron. Eng.*, **130**(1), 111-115. https://doi.org/10.1061/(ASCE)1090-0241(2004)130:1(111).

Krahn, J. (2003), "The 2001 R.M. Hardy Lecture: The limits of limit equilibrium analyses", *Can. Geotech. J.*, **40**, 643-660. https://doi.org/10.1139/t03-024.

Lam, L. and Fredlund, D.G. (1993), "General limit equilibrium model for three-dimensional slope stability analysis", *Can. Geotech. J.*, **30**(6), 905-919. https://doi.org/10.1139/t93-089.

Lee, J.H., Ahn, J.K. and Park, D. (2015), "Prediction of seismic displacement of dry mountain slopes composed of a soft thin uniform layer", *Soil Dyn. Earthq. Eng.*, **79**(A), 5-16. https://doi.org/10.1016/j.soildyn.2015.08.008.

Li, A.J., Merifield, R.S. and Lyamin, A.V. (2009), "Limit analysis solutions for three dimensional undrained slopes", *Comput. Geotech.*, **36**(8), 1330-1351. https://doi.org/10.1016/j.compgeo.2009.06.002.

Lim, K., Lyamin, A., Cassidy, M. and Li, A.J. (2015), "Three-dimensional slope stability charts for frictional fill materials placed on purely cohesive clay", *Int. J. Geomech.*, **16**(2), 04015042. https://doi.org/10.1061/(ASCE)GM.1943-5622.0000526.

Meisina, C. and Scarabelli, S. (2007), "A comparative analysis of terrain stability models for predicting shallow landslides in colluvial soils", *Geomorphology*, **87**, 207-223. https://doi.org/10.1016/j.geomorph.2006.03.039.

Michalowski, R.L. and Drescher, A. (2009), "Three-dimensional stability of slopes and excavations", *Géotechnique*, **59**, 839-850. https://doi.org/10.1680/geot.8.P.136.

Michalowski, R.L. and Martel, T. (2011), "Stability charts for 3D failures of steep slopes subjected to seismic excitation", *J. Geotech. Geoenviron. Eng.*, **137**(2), 183-189. https://doi.org/10.1061/(ASCE)GT.1943-5606.0000412.

Michel, G., Kobiyama, M. and Goerl, R. (2014), "Comparative

analysis of SHALSTAB and SINMAP for landslide susceptibility mapping in the Cunha River basin, southern Brazil", *J. Soils Sediments*, **14**, 1266-1277. https://doi.org/10.1007/s11368-014-0886-4.

Moore, I.D., Grayson, R.B. and Ladson, A.R. (1991), "Digital terrain modelling: A review of hydrological, geomorphological, and biological applications", *Hydrological Processes*, **5**, 3-30. https://doi.org/10.1002/hyp.3360050103.

Naeij, M., Ghasemi, H., Ghafarian, D. and Javanmardi, Y. (2021), "Explicit finite element analysis of slope stability by strength reduction", *Geomech. Eng.*, **26**(2), 133-146. https://doi.org/10.12989/gae.2021.26.2.133.

Newmark, N.M. (1965), "Effects of earthquakes on dams and embankments", *Géotechnique*, **15**, 139-160. https://doi.org/10.1680/geot.1965.15.2.139.

Pantelidis, L. and Griffiths, D. (2013), "Stability of earth slopes. Part II: Three dimensional analysis in closed-form", *Int. J. Numer Anal. Method. Geomech.*, **37**, 1987-2004. https://doi.org/10.1002/nag.2116.

Pantelidis, L., Gravanis, E. and Gkotsis, K.P. (2020), "Stability assessment of soil slopes in three dimensions: The effect of the width of failure and of tension crack", *Geomech. Eng.*, **22**(4), 319-328. https://doi.org/10.12989/gae.2020.22.4.319.

Qi, S., Yand, X.G., Zhou, J.W. and Lu, G.D (2019), "Stability analysis of an unsaturated expansive soil slope subjected to rainfall infiltration", *Geomech. Eng.*, **19**(1), 1-9. https://doi.org/10.12989/gae.2019.19.1.001.

Rao, P., Wu, J., Jiang, G., Shi, Y., Chen, Q. and Nimbalkar, S. (2021), "Seismic stability analysis for a two-stage slope", *Geomech. Eng.*, **27**(2), 189-196. https://doi.org/10.12989/gae.2021.27.2.189.

Reid, M.E., Christian, S.B., Brien, D.L. and Henderson, S.T. (2015), Scoops3D-Software to analyze 3D slope stability throughout a digital landscape, U.S. Geological Survey Techniques and Method.

Saulnier, G.M., Beven, K. and Obled, C. (1997), "Including spatially variable effective soil depths in TOPMODEL", *J. Hydrology*, **202**, 158-172. https://doi.org/10.1016/S0022-1694(97)00059-0.

Shin, H. and Kim, J.W. (2017), "Integrated numerical model for coupled surface-subsurface flow systems", *J. Korean Soc. Hazard*, **17**(6), 201-206. https://doi.org/10.9798/KOSHAM.2017.17.6.201.

Silvestri, V. (2006), "A three-dimensional slope stability problem in clay", *Can. Geotech. J.*, **43**, 224-228. https://doi.org/10.1139/t06-001

Stianson, J.R., Fredlund, D.G. and Chan, D. (2011), "Three-dimensional slope stability based on stresses from a stress-deformation analysis", *Can. Geotech. J.*, **48**, 891-904. https://doi.org/10.1139/t11-006.

Sun, C., Junrui, C., Zengguang, X. and Qin, Y. (2017), "3D stability charts for convex and concave slopes in plan view with homogeneous soil based on the strength-reduction method", *International J. Geomech.*, **17**(5), 06016034. https://doi.org/10.1061/(ASCE)GM.1943-5622.0000809.

Tran, A.T.P., Kim, A.R. and Cho, G.C. (2019), "Numerical modeling on the stability of slope with foundation during rainfall", *Geomech. Eng.*, **17**(1), 109-118. https://doi.org/10.12989/gae.2019.17.1.109.

Tesfa, T., Tarboton, D., Chandler, D. and Mcnamara, J. (2009), "Modeling soil depth from topographic and land cover attributes," *Water Resour. Res.*, **45**, W10438. https://doi.org/10.1029/2008WR007474.

Xie, M., Esaki, T. and Cai, M. (2004), "A GIS-based method for locating the critical 3D slip surface in a slope", *Comput. Geotech.*, **31**, 267-277. https://doi.org/10.1016/j.compgeo.2004.03.003.

Xie, M., Esaki, T., Qiu, C. and Wang, C. (2006), "Geographical information system-based computational implementation and application of spatial three-dimensional slope stability analysis", *Comput. Geotech.*, **33**, 260-274. https://doi.org/10.1016/j.compgeo.2006.07.003.

Yu, H., Salgado, R., Sloan, S. and Kim, J. (1998), "Limit analysis versus limit equilibrium for slope stability", *J. Geotech. Geoenviron. Eng.*, **124**(1), 1-11. https://doi.org/10.1061/(ASCE)1090-0241(1998)124:1(1).

Zhang, F., Leshchinsky, D., Gao, Y. and Yang, S. (2018), "Three-dimensional slope stability analysis of convex turning corners", *J. Geotech. Geoenviron. Eng.*, **144**(6), 06018003. https://doi.org/10.1061/(ASCE)GT.1943-5606.0001896.

GC